Non network-former cations in oxide glasses spotted by Raman scattering

Bernard Hehlen, Daniel R. Neuville

Non network-former cations in oxide glasses spotted by Raman scattering

Bernard Hehlen,[*a] and Daniel R. Neuville,[b]

The depolarized Raman spectra of about 30 binary and ternary aluminosilicate glasses have been collected. Two spectral responses involving the cations are observed below 400 cm^{-1}. One of the two bands arises solely from cations close to non-bridging oxygens. This observation holds for all the glasses investigated providing thereby a simple test for qualifying the polymerization state of oxide glasses. The second feature involves all cations whatever their role in the glass and is found to be twofold: one contribution arises form cations charge compensating AlO$_4^-$ tetrahedra and the other one by network modifier cations. These results confirm the net vibrational contrast of cations depending on their structural surrounding. Finally, while alkali atoms vibrate independently from the rest of the network, alkali-earth cations close to non-bridging oxygens drag the latter in their motion.

1   I. Introduction

Raman scattering is very sensitive to structural modifications in materials and provides in principle a powerful tool for probing the atomic structures. In disordered solids however the vibrational responses are usually broad, dissymmetric, and sometimes overlapping. In addition, the structural disorder often prevents for a selection rule analysis similar to that developed for crystals and molecules. Glasses suffer from these spectroscopic limitations which considerably limit the spectral analyses. Despite, there exists spectral indicators in Raman which provide valuable information on local and medium range structure, some being hardly accessible otherwise. In simple oxide glasses, these are for example the number of threefold and fourfold Si-O-Si rings[1–4], the distribution of SiO$_4^{(4-n)-}$ tetrahedra (so-called Q^n species)[5–7], the Si-O-Si angle distribution in silicates[1,4,8], the amount of BO$_3$ triangles and BO$_4$ tetrahedra in botates[9], among others. Very often though, relating the Raman data to structural numbers deserves calibration with a third party experiment such as NMR, X-Ray diffraction, or numerical simulations.

Vibrations involving the cations are located at low frequency, below 400 cm^{-1} typically and by now have been studied mostly by infrared spetroscopies[10–14]. Interestingly, there exists very few reports on Raman scattering, although cations play a crucial role in the glass, for example when considering the melting temperature, the diffusion processes, the mechanical properties... From a structural point of vu, the cations (M) depolymerize the Si-O-Si connected network by creating ionic bonds with alkali and alkaline-earth units, in which the oxygen ions are called non-bridging oxygens (NBO). In aluminosilicates, when Al is in fourfold coordination it acts as a network former by forming AlO$_4^-$ tetrahedra covalently connected to the silica network. The cations can therefore be either network modifiers as in the previous case, or *charge compensators* when they compensate the negative charge carried by the AlO$_4^-$ tetrahedra. The balance between these two distinct functions varies as a function of the M/Al ratio and controls many of the physical properties of the glass, such as the viscosity.

In a previous report we show that the depolarized Raman spectra of alumino-silicate glasses exhibit two cation bands: a low frequency one around 150 cm^{-1} hereafter called ω_1 and a high frequency one around 330 cm^{-1} hereafter referred to as ω_2.[15] In the two glass families investigated, ω_2 involved only cations at modifier place, while all cations where supposed to contribute to ω_1. The atomic displacements underlying these modes are not yet identified. However, a visual inspection of the vibrations calculated using first principle molecular dynamic simulations suggests that the latter corresponds to a dangling of the Na atom around the oxygen atom to which it is attached[16].

[a] Address, Laboratoire Charles Coulomb (L2C), UMR 5221 CNRS-Université Montepllier, Montpellier, France; Tel: +33 4 67 14 34 64; email : bernard.hehlen@umontpellier.fr

[b] Address, Géomatériaux, IPGP-CNRS, Université de Paris, 1 rue Jussieu, 75005 Paris, France.

The aim of the present work is to investigate a large set of alkali and alkali earth silicate glasses in order to get more insights into the vibrational motions underlying the cations bands, enabeling conclusions which apply over the whole aluminosilicate glass family. To reach this objective, we investigated more than 30 glass compositions, the most prominant series being sets of alcaline-earth aluminosillicates with constant silica content, $50SiO_2$-zMO-yAl_2O_3 and M = Mg, Ca, Sr, Ba, with y varying between 0 to 40 in mole %. The ratio R =MO/Al_2O_3 ranges from 0.25 to infinity and therefore crosses the tectosilicate join at $R = 1$ (Table 1). The glasses contain both modifier and charge compensator cations for compositions in the paralcaline domain ($R > 1$), and only charge compensator cations for compositions in the peraluminate region ($R < 1$), in a simple model assuming all aluminum atoms fourfold coordinated. Sodo-silicates and sodo-aluminosilicates have also been studied to complement these series with alkali-based glasses. The compositions are summarized in Table 1.

Spectroscopic details and sample preparation are shortly described in section II. The spectroscopy in the binary glasses is presented in section III while ternary systems are discussed in detail in section IV. A special attention has been given to the low frequency cation mode which turned to be twofold in the aluminosilates glasses.

2   II. Experimental conditions and sample preparation

The Raman spectra have been recorded using a single pass HR630 Jobin-Yvon diffractometer. The incident light was delivered by a solid state laser working at 532 nm with a linearly polarized beam focused into the sample with a $\times 100$ microscope objective. The polarization of the light scattered in the backscattering geometry was analysed by a half plate wave followed by a broad band Glan-Thomson polarizer while the strong elastic line was rejected using two Bragg filters[17]. To ensure a good reproducibility of the scattered intensities, the irradiated surface of the samples were all flats and polished to optical quality. Finally all spectra were recorded after each other keeping the same experimental conditions.

The samples were obtained by melting mixtures of Na_2CO_3, $CaCO_3$, $SrCO_3$, $BaCO_3$, MgO, Al_2O_3 and SiO_2 (Rectapur from Merck). The mixing was ground for 1 hour under alcohol in an agate mortar, heated slowly to decompose the carbonates, and then heated above the melting point following[18]. The melts were maintained for a few hours at high temperature (1900K for aluminosilicate melt and 1400 K for silicate melt) in air. The sample was quenched in a few seconds from high temperature by dipping the bottom of the platinum crucible into pure water. Peraluminous glasses were obtained by melting a ceramic firstly made at high temperature following previous paper[19–21] respectively for Ca-, Mg-, and Sr-aluminosilicate glasses). The heating procedure was repeated until no crystallization could be detected by optical

microscope and X-ray diffractometry. All materials were found to be chemically homogeneous glassy phases before and after viscosity measurements. Glass sample were analyzed using an electron microprobe analyses, Cameca SX100.

3   III. Binary glasses

3.1   Sodo-silicates: fitting strategy

For sake of data homogeneity, the Raman spectra of the sodosilicates investigated in[15] were recorded again using the same experimental conditions as for all the other glasses studied in this work. The depolarized Raman spectra shown in Figure 1 provides
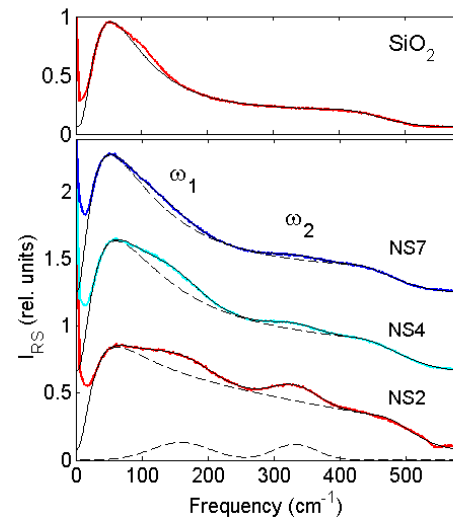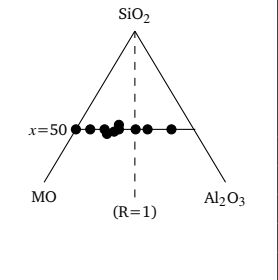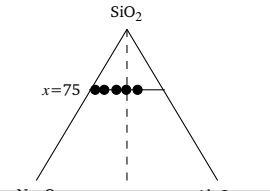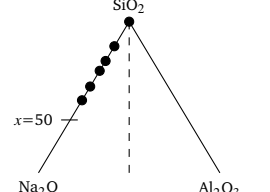

Fig. 1 Depolarized Raman spectra (I_{VH}) of selected sodosilicate glasses and pure silica in the region of the cations modes ω_1 and ω_2. The solid lines result from a fit using a modified lognormal function for the boson peak (see text) and gaussians for the cation modes ω_1 and ω_2 (dashed lines).

examples for describing the fitting procedure. Extracting information on the cation modes deserves fitting simultaneously the boson peak (BP) and its decay at high frequency. The steep increase up to its maximum arises from quasi-local optic vibrations competing with a continuum of acoustic-like excitations. Above the maximum, incoherent scattering from optic modes possibly comes into play giving rise to a sample dependent response.[22,23] Whatsoever the origin, there exists no analytical way to describe this complex spectral shape and one therefore has to find acceptable compromises. In our former paper[15] this signal was modeled by an exponential decay in the frequency region surrounding the high frequency cation mode ω_{2m} around 330 cm^{-1}. We now want to analyse ω_1 at low frequency together with ω_2. This requires fitting a larger spectral range and hence the boson peak as a whole. The model chosen for fitting the boson peak is composed by a lognormal function accounting for its low frequency part, an exponential decay taking over continuously at frequencies above

Table 1 List of glass samples and location in the ternary phase diagram.

Alkaline earth aluminosilicates	M=Mg x-y	M=Ca x-y	M=Sr x-y	M=Ba x-y	
xSiO$_2$:yAl$_2$O$_3$:zMO	50-00	50-00	50-00	50-00	SiO$_2$ / x=50 / MO (R=1) Al$_2$O$_3$
		50-06			
	52-12	50-12	50-12	50-12	
	48-13				
	49-16				
		50-18			
	50-25	50-25	50-25	50-25	
	50-30	50-30	50-30	50-30	
	50-40	50-40	50-40	50-40	

Alkaline aluminosilicates	M=Na x-y	
xSiO$_2$:yAl$_2$O$_3$:zM$_2$O	75-02	SiO$_2$ / x=75 / Na$_2$O Al$_2$O$_3$
	75-05	
	75-09	
	75-12	
	75-16	

Sodo-Silicates	x-z	
xSiO$_2$:zNa$_2$O	100-0	SiO$_2$ / x=50 / Na$_2$O Al$_2$O$_3$
	87.5- 12.5	
	80-20	
	75- 25	
	67-33	
	60-40	

its maximum (above $\sim$150 cm^{-1} typically), and a cutoff with a gaussian decay shape around 450-500 cm^{-1}. This "modified log-normal" function is clearly a rough approximation, but it has the merit of being relatively stable during the fitting procedure, with fitting parameters evolving smoothly and monotoneously from one spectrum to the other, reproducing thereby the evolution of the boson peak. The cation modes ω_1 and ω_2 on top of this signal have been modeled by gaussian functions characterized by their frequency, width, and area. The numerous fitting tests we performed reveal that the output parameters of ω_2 are quite robusts. The reason is that it stands on a relatively flat background in all glasses. The steep and curved slope on which stands ω_1 leads to larger uncertainties, sometimes limiting the spectral analysis.

The superposition of the model (solid line) with the experimental data in sodosilicates (Fig. 1) highlights the good quality of the fits, at least for that glass series. Despite, in pure silica the modified lognormal function is unable to reproduce the bump around 120 cm^{-1}[24]. For some glasses this peculiar shape of the BP is an additional drawback limiting the fitting quality. Therefore, we will only present below the trends of the fitting parameters which are not (or weakly) sensitive to the fitting quality of the boson peak "background" signal. The only exception is the area of ω_1, subject to large uncertainty, but whose behavior turns out to be useful for the discussion. It is finally worth noticing here that the

IR response of ω_1 is most likely bimodal[11,12] but still, we fitted its Raman signature with a single gaussian according to the fact that the proximity of the strong boson peak prevents from a more detailed analysis.

3.2 Alkali earth silicates

ω_1 and ω_2 are also present in alkali-earth silicates as shown in the depolarized Raman spectra of the 50SiO$_2$:50MO glasses with M=Mg, Ca, Sr, and Ba (Figure 2). The responses are intense and can also be observed in experiments performed without polarization analysis. In the latter situation however, the Si-O-Si bending motions (R-band) together with the signal arising from the boson peak drastically confuse the spectral analysis. The arrow in Figure 2a indicates the position of ω_2 in MgSiO$_3$ extrapolated from the three other glasses. It shows that ω_2 is absent (or very weak) in that glass while very strong in the three other compounds. This observation provides an additional evidence that Mg-based silicates behave in a peculiar way as compared to other silicates. For example, they exhibit a highly disordered local structure with a coordination number of $\sim$ 4 to 4.5[20,25,26] significantly lower than for the other alkaline earth cations, between 6 and 8. These effect correlate with the value of the field strength which is the highest for magnesium, bringing the authors to sometimes position this cation as intermediate between glass modifier and glass former.
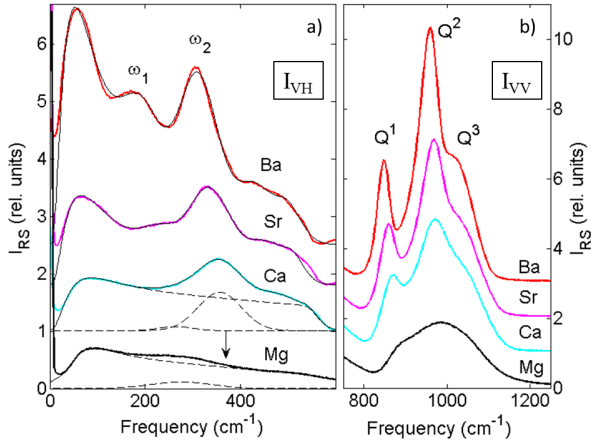
Fig. 2 a) Depolarized Raman spectra (I_{VH}) of $MSiO_3$ glasses ($50MO:50SiO_2$) with M=Mg, Ca, Sr, Ba, and their fits. The arrow indicates the position of ω_2 in $MgSiO_3$ extrapolated from the three other glasses. **b)** Polarized Raman spectra (I_{VV}): zoom on the Q^n bands. For sake of visibility, the spectra have been translated vertically.

These structural specificities are also captured in the Raman response of the Q^n species shown in Figure 2b. The Q^2 and Q^1 bands are rather well defined except in the Mg-based glass where the Q^n feature transforms into a single and very broad structure. This behavior likely results from a pronounced structural disorder at the Si-NBO sites giving rise to ill-defined Si-NBO stretching motions. Finally, the strong disorder close to the Mg cation also explains the very broad response of ω_1 in $MgSiO_3$ (Fig. 2a) as compared to other $MSiO_3$ glasses.
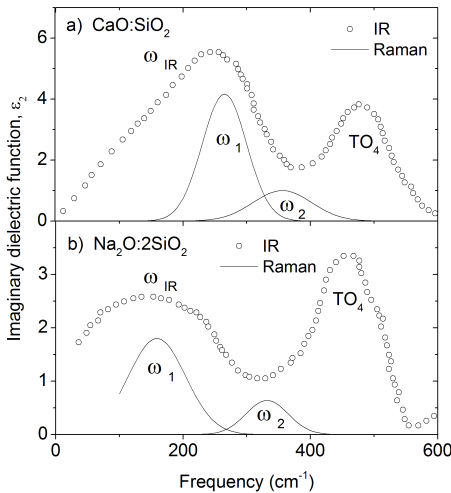

Fig. 3 Comparison between the dielectric function ε_2 measured in IR (circles) and the response of the two cations bands ω_1 and ω_2 extracted from the Raman spectra (lines, see text for details) in **a)** $CaO:SiO_2$[13] and **b)** $Na_2O:2SiO_2$[10].

Figure 3 compares the Raman signature of the cation modes ω_1

and ω_2 with the IR spectra for the binary compounds $CaO:SiO_2$[13] ($CaSiO_3$) and $Na_2O:2SiO_2$[10] ($Na_2Si_2O_3$). ω_2 falls in the deep between the broad feature ω_{IR} assigned to cation motions[12] and the transverse optic mode TO4 around 480 cm^{-1} corresponding to the rocking of the Si-O-Si bonds[27]. ω_1 has a frequency similar to that of ω_{IR} suggesting that both responses correspond to the same type of vibrations. For the reasons mentioned in the preceding section (lack of accuracy owing to the strong boson peak nearby), we preferred to fit ω_{IR} with one single gaussian although the IR data clearly show a structured spectral shape du to different cation environments motivating fitting procedures using two gaussians[12].

For a harmonic oscillator involving n atoms, like *e.g.* a molecule, the eigenfrequencies are given by $\omega_0 = \sqrt{k_c/\mu}$ where k_c is the caracteristic spring constant and μ the reduce mass of the eigenmode under consideration. The frequency of the two IR components building the infrared response ω_{IR} is reproduced in Figure 4. It exhibits a linear behavior when plotted as a function of $\sqrt{1/m_M}$, where m_M is the mass of the cation[12]. Since $\mu = m_M$, this lead the authors to conclude that the modes building ω_{IR} involve solely the cations, *i.e.* in a motion almost independent from their anionic surrounding.
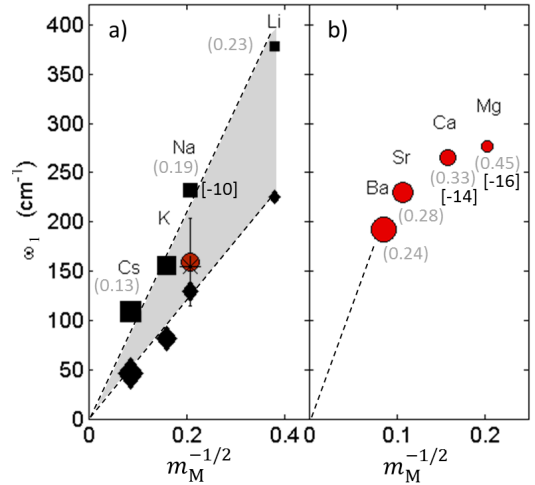

Fig. 4 Frequency of ω_1 in Raman and ω_{IR} in Infrared plotted as function of $\sqrt{1/m_M}$. The size of the symbols refers to the atomic radii of the cations **a)** Alkaline-silicates: The circle is our work, the filled squares and filled losanges correspond to the two-component description of the IR response ω_{IR}[12], and the star is reproduced from[10]. **b)** Alkaline-earth silicates (our work). The numbers in parentheses are the field strengths[28] and those in braquets are $\log_{10}(D)$ where D are the diffusion coefficients compiled from[?].

Lets now consider the case of alkaline-earth silicates (Figure 4b). The frequency ω_1 now deviates from the linear behavior and the effect becomes more pronounced for lighter cations. This different behavior between alkali and alkali earth ions goes along with the increase of the atomic field strengths which are
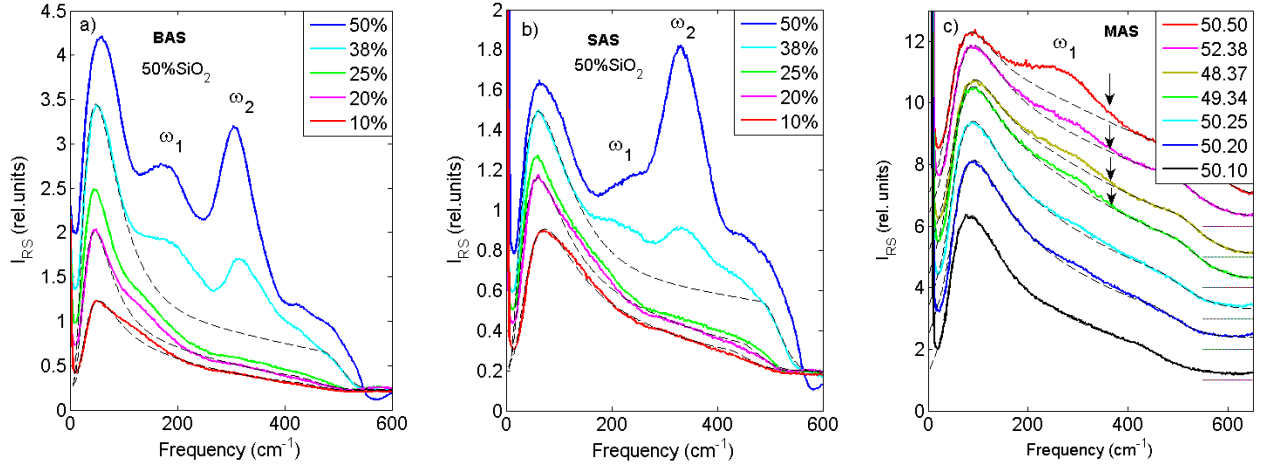
Fig. 5 Depolarized Raman spectra (I_{VH}) of aluminosilictes, $x\mathrm{SiO_2}$:$y\mathrm{Al_2O_3}$:$z\mathrm{MO}$. **a)** M=Ba, with x=50% and z in the legend, **b)** M=Sr, with x=50% and z in the legend, **c)** M=Mg, with the legend in the format $x.z$. Examples of fitted boson peaks are shown to give an idea of the spectral shapes underneath ω_1 and ω_2 (dashed lines). The spectra in Mg-based glasses have been translated-up for sake of clarity. The baselines are given by the horizontal lines on the right. The arrows indicate the expected positon of ω_2 in MAS.

higher for the former. Indeed, when the electrostatic interaction increases, the cation become more and more bonded to the oxygens nearby and drag them along in its motion. The mass of the vibrating structure increases and hence m_M should be replaced by μ.

When considering m_M instead, the curve $\omega = f(\sqrt{1/m_M})$ artificially bends down, exactly as ω_1 does in Figure 4b. The increasing network connectivity for light atoms goes along with a decrease of the cation diffusivity D, revealing in addition the close link between mode frequency, field strength, and diffusivity. This analysis captures the overall motions of the cations : two main vibrations in their cage, ω_1 and ω_2, and the relaxations at high temperature, *i.e* diffusion processes characterized by the diffusion coefficient D.

4 IV. Aluminosilicates

The depolarized Raman spectra of the ternary aluminosilicates series $x\mathrm{SiO_2}$:$y\mathrm{Al_2O_3}$:$z\mathrm{MO}$ with M=Ba, Sr, Mg, are shown in Figure 5. The spectra of calcium glasses are displayed in Figure 4b of Ref.[15]. Surprisingly, the appearance of an additional structural surrounding for the cations in the ternary systems does not translate into additional Raman bands. However, a direct inspection shows that ω_1 is present down to the lowest cation concentration suggesting that the band now gather the motions of both network modifier and charge compensator cations. One also observes that ω_2 vanishes around $z = 25$, that is at the joint $R = 1$ (Ba and Sr glasses) confirming previous anticipations that this band arises solely from cations close to non-bridging oxygens. Similarly to the binary MgO:SiO$_2$ system, ω_2 is still absent (or very weak)

in all of the MgO-aluminosilicates investigated. For this set of glasses the silica content is close but not always equal to 50% and the spectra are displayed by decreasing concentration of MgO to highlight the concomitant intensity decrease of ω_1.

4.1 Low-frequency cation mode ω_1

Figure 6a gather the fitted integrated intensities of ω_1 in the aluminosilicates and sodosilicates series. In calcium glasses ω_1 is embedded under the strong ω_2 band and the fitting parameters could not been exploited (see Fig. 2a). For the other glasses, the relatively large dispersion of the points arises from the fitting limitations mentioned in section III. Despite, when scaling all the intensities on the same value at $z = 25$ ($R = 1$) one clearly observes a change in the slope between peraluminate and paralcaline domains. The effect is more pronounced for heavy cations and likely accounts for a change in the Raman efficiency when network modifiers ($R > 1$) or charge compensators ($R < 1$) are involved.

This and the step increase of the frequency of ω_1 around $R = 1$ shown in Figure 6b suggests a doublet structure of the Raman response : when all cations are charge compensators ([z] < 25, neglecting Al^V or Al^{VI} structures) the frequency ω_1 ($\equiv \omega_{1c}$) is fairly constant and has a different value than ω_1 ($\equiv \omega_{1m}$) for the binary glasses for which all cations are network modifiers ([z] =50). In between, the glasses have both network modifier and charge compensator cations, and the Raman response likely becomes twofold, *i.e.* $\omega_1 = \omega_{1c} + \omega_{1m}$. Unfortunately, the spectroscopy is unable to separate the two contributions, leading to an apparent up-shift (or down-shift in Mg-based glasses) of the frequency when cation oxide is replaced by aluminum oxide. This
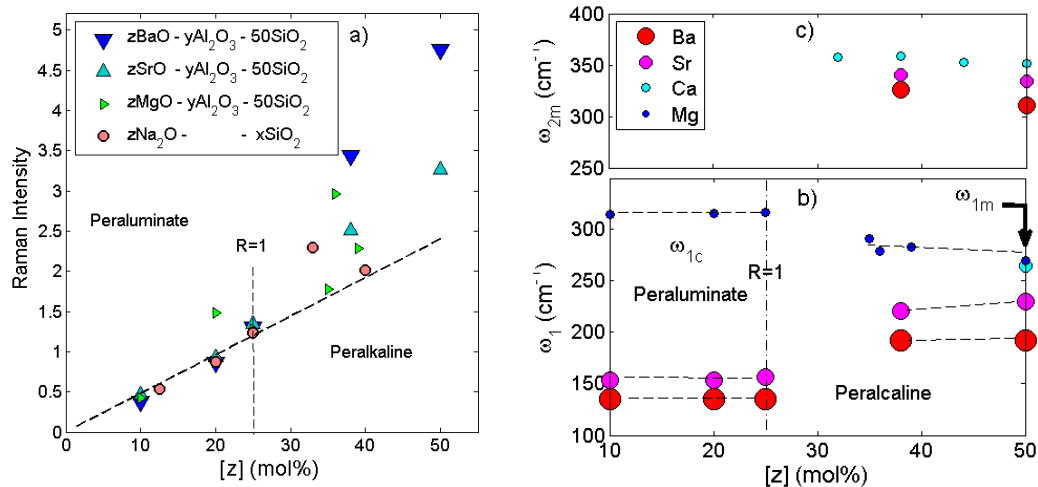
Fig. 6 a) Integrated intensity of ω_1 as a function of the cation content [z]. The data have been scaled to coincide at concentration $z = 25$ ($R = 1$). **b)** and **c)** Frequency of the cations modes ω_1 and ω_2 as a function of [z], respectively.

is however well correlated with the ^{23}Na NMR observed between sodium silicate and aluminosilicate glasses[30] where a NMR chemical shift is observed between charge compensator and network modifier cations, and also with XANES results at the Ca K-edge of CaO-SiO$_2$ and 25CaO-25Al$_2$O$_3$-50SiO$_2$ glasses, where a shift in the XANES pre-edge is observed as a function of the cation site[31].
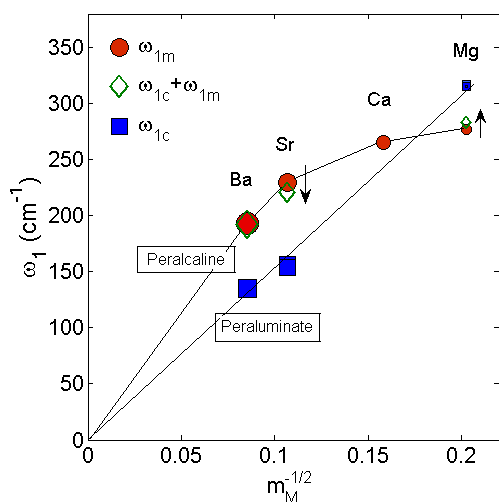

Fig. 7 Frequency of ω_1 as a function of $\sqrt{1/m_M}$ in the aluminosilicate glasses. Red filled circles: binary glasses MOSiO$_3$ ([z]=0); green diamonds: paralkaline glasses ([z]=12%); blue squares: peraluminate glasses, ([z]=25%, 20% and 10%, from dark blue to light blue). In the latter the frequency is similar for the three [z] values and the points superpose. Lines are guide to the eye.

In an attempt to confirm the above assumption we gather in

Figure 7 the curves ω_1(M) as a function of $\sqrt{1/m_M}$ for cations concentrations [z]=10, 20, 25, 38, and 50mol%. The filled circles correspond to the binary silicates, [z]=50 mol%, the empty losanges correspond to aluminosilicates with [z]=38 mol% (peralkaline domain), and the squares to aluminosilicates with [z]= 25, 20 and 10mol% (peraluminate domain). One observes two distinct behaviors. For a predominance of network modifier cations in the glass (peralkaline domain), cation motion couples with the oxygen atoms nearby leading to the observed bending of the frequency dependence of ω_1, as explained in the preceding section. The situation is very different for glasses in the peraluminate domain. In that case, there is only one possible site for the cations, *i.e.* charge compensators, and the three data sets merge in a single straight line meaning that the motion of those cations is now decoupled from the rest of the network. Indeed, the negative charge carried out by the AlO$_4^-$ to which the cation is attached is delocalized leading to a loose directional bonding. Keeping in mind that ω_1 likely results from a dangling motion of the cations, this and the large mass difference between cations and tetrahedra can produce the observed "vibrational decoupling effect". However, although directionally loose, the bonding of the cation to its AlO$_4^-$ tetrahedra should remain strong along the radial axis, as indicated by the weaker value of the diffusion coefficient of charge-compensator cations as compared to network modifiers ones. This result is in line with the IR data of alkaline-earth borate glasses[32] where the authors also found a linear behavior in a plot of ω_{IR} versus $\sqrt{1/m_M}$. For the studied concentration (0.45MO:0.55B$_2$O$_3$) most of the cations compensate BO_4^- tetrahedra[33] which corresponds to a situation similar to the peraluminate domain in alumino silicates. Finally, Table 2 summarizes the values for these three sets of frequencies, *i.e.* ω_{1c}, ω_{1m}, and

ω_2.

Table 2 Frequency of the two cation modes ω_1 and ω_2 in alkaline-earth aluminosilicates (in cm^{-1}): contribution of charge compensator cations ω_{1c} and network modifier cations ω_{1m} to the low frequency response ω_1, and high frequency response ω_2 originating solely from modifier cations and taken at [z]=50.

Cation (M)	ω_1		ω_2
	ω_{1c}	ω_{1m}	
Mg	316	270	-
Ca	-	265	352
Sr	155	230	334
Ba	135	193	310

4.2 High frequency cation mode ω_2

Let's now consider the high frequency mode ω_2. Its frequency and integrated intensity are presented as a function of the cation content in Fig. 6c and 8a, respectively. The latter compiles the data obtained in alkaline-earth aluminosilicates, sodo aluminosilicates, and sodo-silicates glasses. These families define three sets of data highlighted by blue (triangles), pink (filled circles), and yellow (empty circles) background colors. Within the alkaline-earth group (triangles), the intensity of the three glass family has been assigned a multiplication factor and as a consequence, all curves superpose.

As expected, the intensities decrease to zero close to the joint $R = 1$ in all of the ternary glasses. Considering only foufold-coordinated $[Al]^{IV}$ atoms in the glasses, this value is reached for $z = 12.5$ in the sodium aluminosilicate, and $z = 25$ in the alkali earth glasses (arrows in Fig. 8a). By multiplying all the sets by a constant accounting for the cation scattering efficiency, all the curves overlapp into a single one, at least when plotted as a function of $[z]_{mod}$, the molar fraction of modifier cations (Fig. 8b). Within our structural approximation, each couple of AlO_4^- tetrahedra is charge compensated by one alkali earth atom, and the latter reads $[z]_{mod} = (z-y)/atm$, where atm is the number of atoms per mole. When $[z]_{mod}$ becomes low, *i.e.* when the concentration of alumina increases up to the peraluminate region, the intensity of ω_2 reaches zero before the joint $R = 1$ ($[z]_{mod} = 0$) in the alkaline-earth glasses, a behavior also visible in Figure 8a. This observation goes along with an increase of $[Al]^V$ and $[Al]^{VI}$ environments. Compensating these structures requires additional cations which hence are lost as network modifiers, leading to a faster decrease of the intensity of the mode as compared to the linear regime extrapolated from high $[z]_{mod}$ values (dashed line in Figure 8b). However, the effect is rather weak and the experimental errorbars prevent for a comparative analysis between Ca, Sr, and Ba.

5 Conclusion

The Raman spectra of alkaline and alkaline-earth aluminosilicates exhibit two spectral responses involving cation motions. The first one at low frequency, typically around $150\,\mathrm{cm}^{-1}$ (ω_1), is likely twofold though not resolved by our experiment. One component (ω_{1c}) arises from cations compensating the negative charge carried by the AlO_4 tetrahedra. Those cations vibrate independently to the heavy structure to whom they are attached. This decoupling is further amplified by the loose and delocalised electrostatic bonding. The second component (ω_{1m}) involves cations at modifier's place, that is attached to non-bridging oxygens. In alkaline-earth alumino silicate glasses the cations drag the NBOs nearby in a coupled motion, a situation different than for alkali cations where the vibration is defined solely by the motion of the cation. A likely explanation is the difference of strength fields which are significantly higher for alkali earth cations. The second cation band appears around $330\,\mathrm{cm}^{-1}$ (ω_2). In aluminosilicates the analysis shows that whatever the cation type, only those at modifier's place contribute to that vibrational response. Overall, these results point-out a clear vibrational contrast between the cations attached to NBOs and those close to AlO_4 tetrahedra. The presence or not of ω_2 in a Raman spectra also provides a simple test for qualifying the polymerization state of a glass. Since responses at similar frequencies appear in the Raman spectra of borate and borosilicate glasses these conclusions likely hold also in these systems.
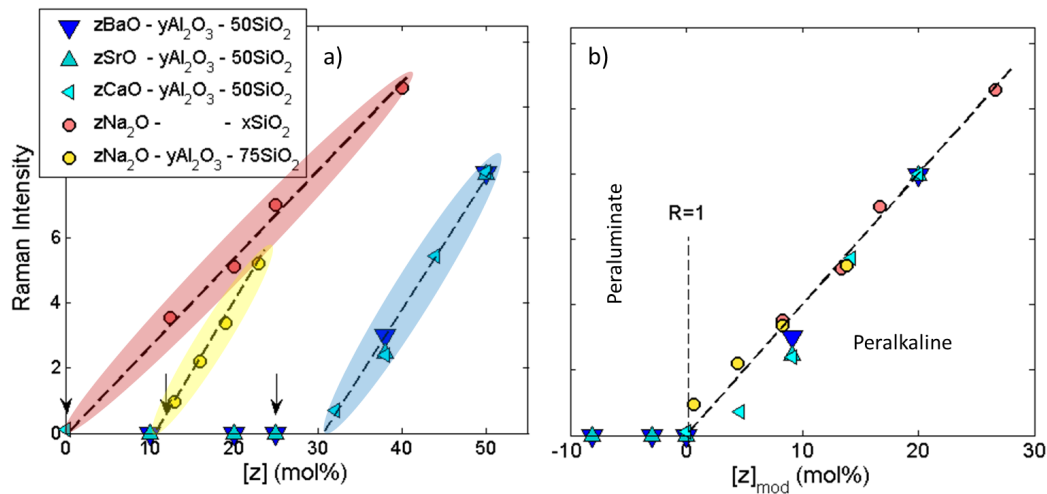
Fig. 8 Integrated intensity of ω_2 **a)** as a function of the total cation content $[z]$ and **b)** as a function of the modifier cation content $[z]_{mod}$. The arrows indicate the join $R = 1$.

Notes and references

1 F.L. Galeener and J.C. Mikkelsen Jr, Vibrational dynamics in ^{18}O-substituted vitreous SiO_2. *Phys. Rev. B*, 1981, **23**, 5527-5530.

2 F.L. Galeener, Planar rings in glasses *Solid State Commun.*, 1982, **44**, 1037-1040.

3 A. Pasquarello and R. Car, Identification of Raman defect lines as signatures of ring structures in vitreous silica *Phys. Rev. Lett.*, 1998, **80**, 5145-5147.

4 B. Hehlen, Inter-tetrahedra bond angle of permanently densified silicas extracted from their Raman spectra. *J. Phys.: Condens. Matter*, 2010, **22**, 025401.

5 P.F. McMillan, Structural studies of silicate glasses and melts-applications and limitations of Raman spectroscopy. *Am. Mineral.*, 1984, **69**, 622-644.

6 B.O. Mysen and J.D. Frantz, Structure and properties of alkali silicate melts at magmatic temperatures. *Eur. J. Mineral.*, 1993, **5**, 393-407.

7 B.O. Mysen, Experimental, in situ, high-temperature studies of properties and structure of silicate melts relevant to magmatic processes. *Eur. J. Mineral.*, 1995, **7**, 745-766.

8 B. Hehlen, D.R. Neuville, D. Kilymis and S. Ispas, Bimodal distribution of Si–O–Si angles in sodo-silicate glasses *J. Non-Cryst. Solids*, 2017, **469**, 39-44.

9 F. Angeli, O. Villain, S. Schuller, T. Charpentier, D. De Ligny, L. Bressel and L. Wondraczek, Effect of temperature and thermal history on borosilicate glass structure. *Phys. Rev. B*, 2012, **85**, 054110.

10 C.I. Merzbacher and W.B. White, Structure of Na in aluminosilicate glasses: A far-infrared reflectances spectroscopics

study. *Am. Mineral.*, 1988, **73**, 1089.

11 E.I. Kamitsos, A.P. Patsis and G.D. Chryssikos, Infrared reflectance investigation of alkali diborate glasses. *J. Non-Cryst. Solids*, 1993, **152**, 246.

12 E.I. Kamitsos and G.D. Chryssikos, Alkali sites in glass. *Solid State Ionics*, 1998, **105**, 75-85.

13 D. De Sousa Meneses, M. Malki and P. Echegut, Optical and structural properties of calcium silicate glasses. *J. Non-Cryst. Solids*, 2006, **352**, 5301.

14 D. De Sousa Meneses, M. Eckes, L. Del Campo, C.N. Santos, Y. Vaills and P. Echegut, Investigation of medium range order in silicate glasses by infrared spectroscopy. *Vib. Spectrosc.*, 2013, **65**, 50.

15 B. Hehlen and D.R. Neuville, Raman response of network modifier cations in alumino-silicate glasses. *J. Phys. Chem. B*, 2015, **119**, 4093-4098.

16 D. Kilymis, S. Ispas, B. Hehlen, S. Peuget and J.-M. Delaye, Vibrational properties of sodosilicate glasses from first-principle calculations *Phys. Rev. B*, 2019, **99**, 054209.

17 OptiGrate Corp.: http://www.optigrate.com.

18 D.R. Neuville, Viscosity, structure and mixing in (Ca, Na) silicate melts. *Chem. Geol.*, 2006, **229**, 28-42.

19 D.R. Neuville, L. Cormier and D. Massiot, Al speciation in calcium aluminosilicate glasses: A NMR and Raman spectrocospie. *Chem Geol.*, 2006, **229**, 173-185.

20 D.R. Neuville, L. Cormier, V. Montouillout, P. Florian, F. Millot, J.-C. Rifflet and D. Massiot, Structure of Mg and Mg/Ca aluminosilicate glasses: ^{27}Al NMR and Raman spectroscopy investigations. *Am. Mineral.*, 2008, **93**, 1721-1731.

21 A. Novikov, D.R. Neuville, L. Hennet, D. Thiaudière, Y. Gueguen and P. Florian, Al and Sr environment in tectosili-

cate glasses and melts: viscosity, Raman and NMR investigation. *Chemical Geology*, 2017, **461**, 115-127.

22 H. Mizuno, H. Shiba and A. Ikeda, Continuum limit of the vibrational properties of amorphous solids, *Proc. Natl, Acad. Sci.*, 2017, **114**, 055902.

23 Y.M. Beltukov, C. Fusco, D.A. Parshin and A. Tanguy, Boson peak and Ioffe-Regel criterion in amorphous silicon-like materials: effect of bond directionality, *Phys. Rev. E,* 2016, **93**, 023006.

24 C. Weigel, M. Foret, B. Hehlen, M. Kint, S. Clément, A. Polian, R. Vacher and B. Rufflé, Polarized raman spectroscopy of v-SiO$_2$ under rare-gas compression. *Phys. Rev. B*, 2016, **93**, 224303.

25 S. Sen, H. Maekawa and G.N. Papatheodorou, Short-range structure of invert glasses along the pseudo-binary join MgSiO$_3$-Mg$_2$SiO$_4$: results from ^{29}Si and [25]Mg MAS NMR spectroscopy. *J. Phys. Chem. B*, 2009, **113**, 15243-15248.

26 L. Cormier and G.J. Cuello, Mg coordination in a MgSiO$_3$ glass using neutron diffraction coupled with isotopic substitution. *Phys. Rev. B*, 2011, **83**, 224204.

27 C.T. Kirk, Quantitative analysis of the effect of disorder-induced mode coupling on infrared absorption in silica. *Phys. Rev. B*, 1988, **38**, 1255.

28 A.H. Dietzel, On the so-called mixed alkali effect. Phys. chem. Glas. *Phys. Chem. Glas.*, 1983, **23**, 172-180.

29 V. Magnien, D.R. Neuville, L. Cormier, J. Roux, J.-L. Hazemann, D. de Ligny, S. Pascarelli, I. Vickridge, O. Pinet P. and Richet, Kinetics and mechanisms of iron redox reactions in silicate melts: The eects of temperature and alkali cations. *Geochim. Cosmochim. Acta*, 2008, **72**, 2157-2168.

30 C. Le Losq, D.R. Neuville, P. Florian, G.S. Henderson and D. Massiot, The role of Al^{3+} on rheology and structural changes in sodium silicate and aluminosilicate glasses and melts. *Geochimica et Cosmochimica Acta*, 2014, **126**, 495-517.

31 M.R. Cicconi, D. de Ligny, T.M. Gallo and D.R. Neuville, Ca Neighbors from XANES spectroscopy: a tool to investigate structure, redox and nucleation processes in silicate glasses, melts and crystals. *American Mineralogist*, 2016, **101**, 1232-1236.

32 Y.D. Yiannopoulos, G.D. Chryssikos and E.I. Kamitsos, Structure and properties of alkaline earth borate glasses. *Phys. Chem. Glasses*, 2001, **42**, 164-72.

33 W.J. Dell, P.J. Bray and S.Z. Xiao, ^{11}B NMR studies and structural modeling of Na$_2$0-B$_2$O$_3$-SiO$_2$ glasses of high soda content. *J. non-Cryst. Solids* 1983, **58**, 1-16.